RESIDUL PERFORMANCE OF REINFORCED CONCRETE COLUMNS UNDER BLAST LOADING

H. Choi[1*], M.S. Kim[1], E. Jo[1], H. Kim[1], D.J. Kim[1] and Y.H. Lee[1†]

[1]*Department of Architectural Engineering, Kyung Hee University, Korea*

ABSTRACT

Failure modes of concrete structure due to blast load vary according to the point of detonation, stand-off distance and TNT charge weight. Especially columns are the key load bearing elements in concrete frame structures. They are typically weak not to long distance explosive loadings but to short distance loadings. In this study, the effect of blast loadings occurred within the short distance was analytically examined. Scaled distance which considers both stand-off distance and TNT charge weight and various arrangement of longitudinal reinforcements with the same sectional area were considered as variables in order to evaluate damage levels and define the relations among these variables with respect to residual strength of columns after blast. AUTODYN was used for the FE analysis. As results, denser arrangement of the longitudinal reinforcements using smaller diameter bars showed relatively better residual capacity.

Keywords: Blast, Reinforced concrete, Columns, Residual strength

1. INTRODUCTION

The potential for structural collapse must be based on assessing local damage of critical structural components, such as columns, girders, and load bearing walls. Explosion causes local structural component damage directly, and damaged structural component can induce global damage of structural system, such as progressive collapse. The effects of two parameters(including arrangement of longitudinal reinforcement, scaled distance) on residual load carrying capacity of reinforced column under explosive loading is studied in this paper. Numerical model was prepared using AUTODYN to predict blast loading and corresponding structural damage. Analytical model

1.1. Blast loadings

Loading environments produced by explosive devices include fragments and the blast wave. In most cases, a cased explosive device is used rather than a bare explosive charge, and causes more severe damage. The combination of pressure and fragment impulse affecting structural damage is not clearly understood yet. Thus, structural damage only from blast is considered in this study.

* Presenter: Email: choihs@khu.ac.kr

† Corresponding author: Email: leeyh@khu.ac.kr

Detonation of explosive produces shock wave as shown in Figure 1, where P_{so} is peak incident pressure, P_0 is ambient pressure, t_0 is duration of positive overpressure, t_o^- is duration of negative overpressure, and is positive specific impulse. The peak incident pressure can be determined by scaled distance Z as expressed in equation (1).

$$Z = R / W^{1/3} \tag{1}$$

where R is standoff distance, and W is equivalent TNT weights.

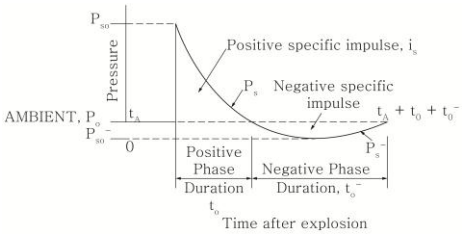

Figure 1: Free-field pressure-time variation (TM 5-855-1, 1986)

1.2. Material models

1.2.1. Concrete

The RHT model has three limit surfaces ; the initial elastic yield surface, the failure surface and the residual friction surface. While the surfaces account for reduction in strength along not only strain rate effects but also different meridians, the static compressive meridian surfaces are depicted in Figure 2. The failure surface consists of material parameters, such as the compressive, tensile and shear strength of the concrete. The initial yield surface consists of user input fractions of the failure surface along the tensile and compressive meridian. And it additionally includes a cap that closes at the current pore crush pressure. A typical loading scenario can be illustrated as follow, see also in Figure 2.

1.2.2. Reinforcement

To describe the behaviour of the reinforcing steel, a piecewise linear Johnson-Cook material model was used, including strain hardening but not strain-rate and thermal effects. This model is a modification to the Johnson-Cook model, where the dependence on effective plastic strain represented by the $A + B\varepsilon_p^n$ from equation (2) is replaced by a piecewise linear function of yield stress Y versus effective plastic strain. Figure 3 shows yield stress of Johns-Cook model. The strain rate dependence and thermal softening terms remain the same as in the Johnson-Cook model. Figure 4 shows yield stress versus effective plastic strain of Piecewise linear Johnson-Cook material model.

$$Y = \left|A + B\varepsilon_p^n\right\|1 + C\ln\varepsilon_p^*\left\|1 - T_H^m\right| \tag{2}$$

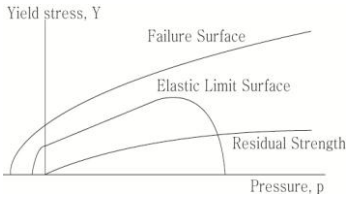

Figure 2: The RHT model used for concrete (Riedel et al., 2000)

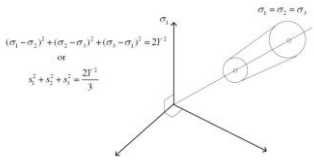

Figure 3: Yield stress of Johnson-Cook Model

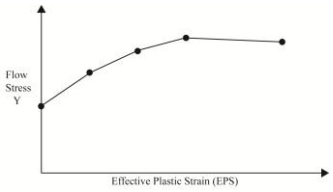

Figure 4: Yield stress versus effective plastic strain of Piecewise linear Johnson-cook model

1.3. Validation

The analytical methodology was validated comparing pressure-history from detonation and maximum deflection with the experimental result from Bing Li et al. (2010). 100 kg of TNT or equivalent was detonated at standoff distance of 5 m, and pressure history and acceleration were measured at the midspan and near support.

Although peak pressure difference is about 16%, difference of impulses is less than 2%, and the shapes of pressure history are similar (Figure 5). Thus, AUTODYN seems to be able to calculate reasonably accurate loading condition. The difference of maximum deflection is 20%, caused by peak pressure underestimation and uncertainty of concrete beam characteristics. Again, deflection histories (Figure 6) are similar, and AUTODYN could give reliable results. Based on these comparisons, analytical methodology described in this section can be used for the parametric study.

Table 1: Differences in pressure characteristics and structural response

	From Bing Li et al. (2010) [A]	From AUTODYN [B]	Difference [(A-B)/A]
Peak Pressure (kPa)	6818 kPa	5726 kPa	16(%)
Impulse (kPa-ms)	3401 kN-ms	3361 kN-ms	1(%)
Maximum displacement(mm)	60 mm	48 mm	20(%)

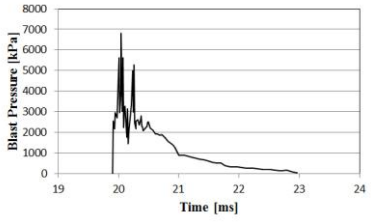

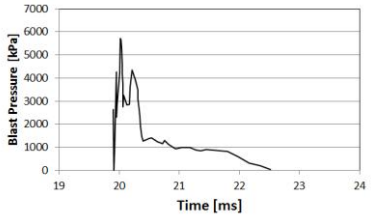

(a) Bing Li et al. (2010) **(b) AUTODYN**

Figure 5: Pressure history

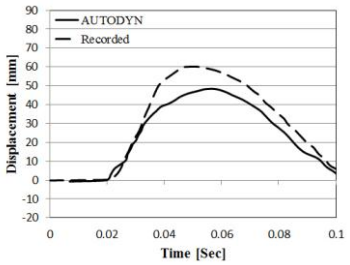

Figure 6: Deflection histories

2. PARAMETRIC ANALYSIS

2.1. Blast loadings and geometry

The analysis consists of three stages: pre blast loading, blast loading, post blast loading stages as shown in Figure 7.

In pre blast loading stage, numerical model for reinforced concrete column and blast loading is prepared with Lagrangian and Euler, respectively. Column has fixed-fixed supports, except that top of column is free to move in axial direction. Constant axial load is applied to the column, which is 20% of the static load carrying capacity.

In blast loading stage, damage and structural response of column under blast loading is simulated. Axial loading remains constant as 0.2 P_n throughout this stage. Simulation continues until blast loading disappears and column does not move due to material damping.

In post blast loading stage, axial force applied on the damaged column increases statically from 0.2 P_n until the column fails. The maximum axial force is treated as the residual load carrying capacity, P_r.

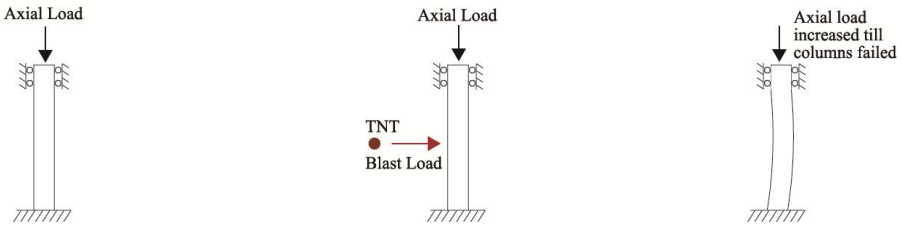

(a) Pre blast loading stage (b) Blast loading stage (c) Post blast loading stage

Figure 7: Analysis procedure

2.2. Variables

Arrangement of longitudinal reinforcement, scaled distance were selected as key parameters affecting residual load carrying capacity. Table 2, Figure 8 shows the parameter values and cross sections, respectively. Each case can be summarized as below:

- 5 cases with different arrangements of longitudinal reinforcement by increasing reinforcement size and reducing number of reinforcements (reinforcement ratio is in the range between 1.90 and 1.99)
- 8 cases with different scaled distances.

All of the columns have D10 lateral reinforcement with 200mm spacing. 35MPa RHT model was used for concrete. Tensile strength of concrete was set as 3.5MPa. 400MPa Piecewise Linear Johnson-Cook model was used for reinforcement.

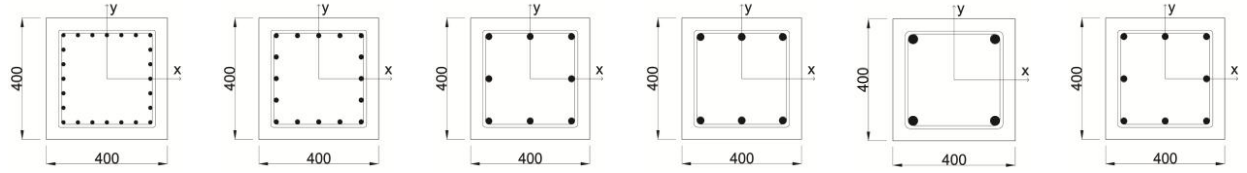

(a) ALR-24 (b) ALR-16 (c) ALR-8 (d) ALR-6 (e) ALR-4 (f) SD Serieses

Figure 8: Cross section

Table 2: Parameter table

Type	Variable	Reinforcement		TNT		Longitudinal Reinforcement Ratio	Scaled Distance [m/kg$^{1/3}$]	P_n
		Longitudinal	Transverse	Mass [kg]	Distance [m]			
ALR-24	Arrangement of Longitudinal Reinforcement	24-D13	D10@200	500	5	1.90	0.63	5885.86
ALR-16		16-D16	D10@200	500	5	1.99	0.63	5936.51
ALR-8		8-D22	D10@200	500	5	1.94	0.63	5906.59
ALR-6		6-D25	D10@200	500	5	1.90	0.63	5885.63
ALR-4		4-D32	D10@200	500	5	1.99	0.63	5936.21
SD-0.85	Scaled Distance	8-D22	D10@200	200	5	1.94	0.85	5906.59
SD-0.75		8-D22	D10@200	300	5	1.94	0.75	5906.59
SD-0.63		8-D22	D10@200	500	5	1.94	0.63	5906.59
SD-0.56		8-D22	D10@200	700	5	1.94	0.56	5906.59
SD-0.45		8-D22	D10@200	300	3	1.94	0.45	5906.59
SD-0.38		8-D22	D10@200	500	3	1.94	0.38	5906.59
SD-0.34		8-D22	D10@200	700	3	1.94	0.34	5906.59
SD-0.23		8-D22	D10@200	700	2	1.94	0.23	5906.59

2.3. Effect of arrangement of longitudinal reinforcement

With the same cross section area and reinforcement ratio, effect of arrangement of longitudinal reinforcement on residual load carrying capacities were analysed. Although lateral stiffnesses of ALR-4 and ALR-6 are higher than ALR-8, ALR-24 and ALR-28, the strain energy absorption increases as number if longitudinal reinforcement increases as shown in Figure 9. Ductility can be improved throughout the cross section of column as number of longitudinal reinforcement increases, thus the increased number is beneficial to resist the blast loading.

2.4. Effect of scaled distance

With the same cross section area and reinforcement ratio, the effect of scaled distance on residual load carrying capacities was analysed. Figure 10 show increase ratios of load carrying capacity. SD-0.85 shows 76% as load carrying reduction, and SD-0.23 has 35% of nominal axial strength as residual load carrying capacity after blast events. Thus residual load carrying capacity increase as the scaled distance increases, and the relationship between R and scaled distance is a rising curve.

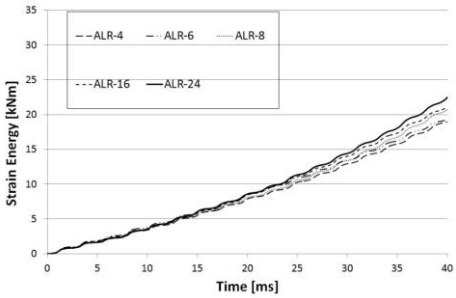

Figure 9: Effect of arrangement of longitudinal reinforcement on strain energy

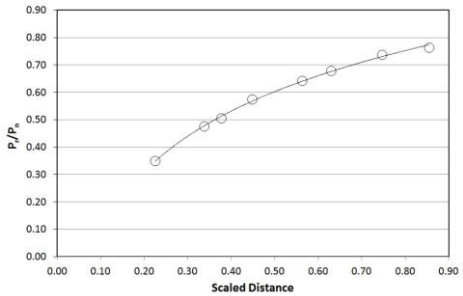

Figure 10: Relationship between reduction ratio of load capacity and scaled distance

3. CONCLUSIONS

In this study, Numerical model was prepared using AUTODYN to predict blast loading and corresponding structural damage. Arrangement of longitudinal reinforcement and scaled distance were selected as key parameters affecting residual load carrying capacity. The following conclusions can be made:

1) The analytical methodology was validated comparing pressure-history from detonation and maximum deflection with the experimental result from Bing Li et al. (2010). Based on these comparisons, AUTODYN seems to be able to calculate reasonably accurate loading condition. And analytical methodology can be used for the parametric study.

2) Ductility can be improved throughout the same cross section area and reinforcement ratio of column as number of longitudinal reinforcement increases, thus the increased number is beneficial to resist the blast loading. Residual load carrying capacity, where residual capacity slightly increases as number of reinforcement increases.

3) The relationship between R and aspect ratio, reinforcement ratio is linear in the scope of simulated columns. But, the relationship between R and scaled distance is a rising curve. This relationship is extremely valuable to predict damages of reinforced concrete structures on the blast.

ACKNOWLEGEMENTS

This work was supported by the National Research Foundation of Korea(NRF) grant funded by the Korea government(MEST) (No. 2012-0005424).

REFERENCES

Bing Li, Zhi Wei Huang, and Chee leong lim (2010), Verification of nondimensional energy spectrum-based blast design for reinforced concrete members through actual blast tests, Journal of Structural Engineering, 136(6), pp. 627-636

Dunnett, J., Flynn, D., and Wharton, J. (2006), Blast Algorithm Development: Definition of Modified Blast Algorithms for PBX Based Explosives, Insensitive Munitions and Energetic Materials Technical Symposium (IMEMTS`06), Bristol, pp. 1-10

Krauthammer, T. (2008), Modern Protective Structures, CRC Press.

Krauthammer, T., Astarlioglu, S. and Blasko, J.R. (2008), Pressure-impulse diagrams for the behavior assessment of structural components, International Journal of Impact Engineering, 35(8), pp. 771-783.

Krauthammer, T., Shahriar, S. and Shanaa, H.M. (1990), Response of RC elements to severe impulsive loads, Journal of Structural Engineering, 116(4). pp. 1061-1079.

Park, J.Y. and Krauthammer, T. (2008), Beam-girder interactions for roof damage analysis under explosive loading, The Proceedings of 4th International Conference on advances in structural engineering and mechanics (ASEM`08), Jeju Island,

PDC-TR 06-01 (2006), Methodology manual for the single-degree-of-freedom blast effects design spreadsheets, US Army Corps of Engineers.

PDC-TR 06-08 (2006), Single degree of freedom structural response limits for antiterrorism design, US Army Corps of Engineers.